https://doi.org/10.1007/s41230-025-4182-2

Influence of final sintering temperature on properties of nano-ZrO_2 reinforced SiO_2-based ceramic cores via stereolithography additive manufacturing

Qi-qi Huang[1], *Chao-yue Chen[1], Yu-hao Yin[1], **Song-zhe Xu[1], Xia Li[1], Tao Hu[1], Shuo Yin[2, 3], Jiang Wang[1], Wei-dong Xuan[1], and Zhong-ming Ren[1]

1. State Key Laboratory of Advanced Special Steels, School of Materials Science and Engineering, Shanghai University, Shanghai 200444, China

2. Trinity College Dublin, the University of Dublin, Department of Mechanical, Manufacturing and Biomedical Engineering, Parsons Building, Dublin 2, Ireland

3. College of Mechanical Engineering, Yangzhou University, Yangzhou 225127, Jiangsu, China

Abstract: As a reliable additive manufacturing technology, the stereolithography (SLA) ceramic core necessitates a tailored sintering process to achieve optimal performance. This study explored the effects of final sintering temperatures (specifically 1,150, 1,250, and 1,300 °C) on the properties of SLA-fabricated SiO_2-based ceramic cores reinforced with nano-ZrO_2 (at concentrations of 1.0wt.%, 1.5wt.%, and 2.0wt.%). The results demonstrate that increasing the final sintering temperature and the incorporation of nano-ZrO_2 enhance the viscous flow of quartz glass, resulting in a higher sintering degree. As the final sintering temperature rises, the ceramic samples exhibit increased shrinkage rate, decreased apparent porosity, and increased bulk density. Higher final sintering temperatures also promote greater cristobalite precipitation, promoting an increase in the amount and precipitation rate of quartz during investment casting. The formation of a cristobalite and $ZrSiO_4$ network at elevated temperatures effectively inhibits the viscous flow of quartz glass, thereby significantly improving high-temperature flexural strength and creep resistance of ceramic cores. When the content of nano-ZrO_2 is between 1.5wt.% and 2.0wt.%, the final sintering temperature of 1,250 °C is the best choice. Under these conditions, the shrinkage rate along the *Z* direction ranges from 3.35% to 3.68%, the porosity lies between 25.57% and 26.03%, the bulk density varies from 1.612 to 1.645 g·cm^{-3}, the room temperature flexural strength is between 26.79 and 27.85 MPa, and the flexural strength at high temperatures is within the range of 30.77 to 33.02 MPa. The deflection at high-temperatures is 3.37–5.31 mm, while the surface roughness of the upper surface is 3.26–4.79 μm, and the surface roughness of the side surface is 4.97–5.79 μm. These findings provide valuable guidance for optimizing the sintering processes of SLA ceramic cores, offering potential for industrial applications.

Keywords: ceramic core; nano-ZrO_2; stereolithography; final sintering temperature; mechanical performance

CLC numbers: TG221 **Document code:** A **Article ID:** 1672-6421(2025)05-519-15

***Chao-yue Chen**

Born in 1987, Ph. D., Associate Professor, Doctoral Supervisor. His research interests primarily focus on the microstructure and performance control of metal additive manufacturing and investiment casting of superalloys.

E-mail: cchen1@shu.edu.cn

****Song-zhe Xu**

Ph. D., Lecturer. Research interests: Computational modeling in fluid mechanics, metal solidification, and forming processes for laser additive and precision manufacturing.

E-mail: songzhex@shu.edu.cn

Received: 2024-11-04; Revised: 2024-11-28; Accepted: 2024-12-02

1 Introduction

Ni-based single-crystal superalloy turbine blades serve as a critical component in modern jet engines, significantly enhancing performance through their exceptional improved high-temperature resistance and superior mechanical properties[1-3]. The capacity to endure higher temperatures directly correlates with an increase in turbine inlet temperatures, thereby boosting the thrust and power output of the engine[4, 5]. In addition to alloy composition and thermal barrier coatings,

advanced cooling technologies have become increasingly crucial for enhancing high-temperature performance and prolonging the service life of turbine blades[6]. For example, the complex internal cooling channels are designed within the inside of the Ni-based single-crystal superalloy blades to facilitate the flow of cooling air, effectively removing heat from the blades[7]. As the internal air-cooling structure becomes more and more complex, the preparation of turbine blades by investment casting requires ceramic cores with complex geometries and high precision[8-10]. Currently, lost-wax inveatment casting has bcome the standard for fabricating superalloy turbine blades[11,12]. tHowever, the traditional preparation techniques for ceramic cores ,such as hot injection molding, have presented significant drawbacks interms of dimensional accuracy, surface quality, design complexity, process labor-intensitve and time-consuming, as well as the incressed production cost[13-15]. Additive manufacturing technology, also known as 3D printing, has become an important technology for preparing complex ceramic cores. It exhibits advantages such as mold-free manufacturing, high precision, and rapid preparation speed[8, 13, 14, 16]. The main additive manufacturing techniques for ceramic cores include selective laser sintering (SLS)[17-20], stereolithography appearance (SLA)[21-24], and digital light processing (DLP)[25-28]. Among all these ceramic additive manufacturing technologies, SLA is the most promising one due to its high preparation accuracy, good surface quality, and a wide range of applicable sizes[13, 22, 29, 30].

It is of great significance to further study the SLA ceramic cores and explore their internal influence mechanism, as this can contribute to the advancement of modern aviation technology. For the moment, the research on ceramics prepared by SLA mainly focuses on the composition of mineralizers and their effects. For example, Chen et al.[31] fabricated porous Al_2O_3-based ceramics with an average pore size of 15 μm via stereolithography. The porosity of the ceramics reached 47.93% and the room temperature flexural strength was 37.89 MPa. The flexural strength of the ceramic sample was further enhanced to 51.36 MPa with nano-Al sol strengthening. Zheng et al.[32] studied the effect of SiC fiber on the properties of SiO_2-based ceramic cores prepared via SLA, and found that an increase of SiC fiber can decrease the linear shrinkage of ceramic cores. The core boasts a flexural strength of 23.83 MPa at room temperature and an impressive 34.62 MPa at high temperatures, fully satisfying the stringent requirements for hollow blade cores. Wang et al.[11] added nano-SiO_2 powder into the Al_2O_3-based ceramic cores, and found that nano-SiO_2 can increase density and creep resistance. The added nano-silica powder is uniformly distributed among ceramic particles, which not only enhances the powder's flowability but also leads to improvements in surface quality, flexural strength, and linear shrinkage. It is reported that the particle size distribution can significantly affect the properties of the ceramic cores[33], and when utilizing nano-sized powders in the fabrication of SLA ceramic green bodies, lower final sintering temperatures are required[34]. To obtain high-quality ceramic cores, preparing a ceramic slurry with a high solid content, low viscosity, high reactivity, and low sedimentation is a very important step[35]. However, the sintering process is also a critical factor that affects the transformation of the ceramic cores from a green body to a ceramic core sample.

Sintering is the key step affecting the comprehensive performance and dimensional accuracy of SLA ceramic cores. The evolution of the ceramic microstructure during the sintering process has a significant impact on their anisotropy[36, 37]. Various factors, including the sintering method, heating rate, final sintering temperature, and holding time, all contribute to these differences in microstructure and, consequently, anisotropy. During the sintering process, the ceramic particles can form a sintering neck and join together to form a strong core part. Qian et al.[36] prepared Al_2O_3 ceramics via SLA and found that different sintering agents had different effects on properties of ceramic cores, in which the addition of 3wt.% CaO promoted the internal porous structure at high temperatures and increased the possibility of interlayer micro-cracks along the internal pores. The addition of 0.5wt.% TiO_2 had the best effect on the room temperature flexural strength of Al_2O_3-based ceramics. La_2O_3 can improve the high-temperature strength of Al_2O_3 ceramics but has no effect on grain refinement. ZrO_2 improved apparent porosity and interlayer shear strength and reduces sintering shrinkage by approximately 30% while maintaining flexural strength. Yang et al.[37] found that with the increase of holding time during the sintering process, the densification degree of Al_2O_3 ceramics became higher and higher, the participating pores gradually disappeared, and the grain size increased. Li et al.[38] explored the effect of the final sintering temperature on the performance of photocurable SiO_2-based ceramic cores. When the final sintering temperature increased from 1,100 °C to 1,300 °C, the precipitation amounts of cristobalite gradually increased. An et al.[39] prepared a SiO_2-based ceramic core by adding ZrO_2 as a mineralizing agent through SLA technology, and observed that ZrO_2 reacted with SiO_2, the base material of the ceramic core, to produce $ZrSiO_4$ when the temperature exceeded 1,350 °C, which enhanced the high-temperature performance of the ceramic cores. Zhang et al.[40] studied the effects of TiO_2 and MgO on the sintering properties of Al_2O_3 ceramic via stereolithography, and concluded that TiO_2 can form a solid solution with Al_2O_3, resulting in main lattice distortion and cation vacancy, thus activating the lattice and promoting solid-state sintering. MgO can form a liquid phase with Al_2O_3 at high temperatures to improve system fluidity and reduce final sintering temperatures. Generally speaking, the final sintering temperature and its holding time are the key parameters in determining the sintering quality and final performance of ceramics. Excessively high final sintering temperature can lead to coarsened grain size, reduced porosity, and occurrence of shrinkage deformation or crack defects. Conversely, at an insufficiently low final sintering temperature, the adhesion among the ceramic powders may be weakened, resulting in poor mechanical properties. Thus, the final

sintering temperature of the SLA ceramic core needs to be determined according to the type of matrix material and the added mineralizing agent[41].

In our previous work, we have demonstrated that the SLA nano-ZrO_2 reinforced SiO_2-based ceramic cores exhibited excellent comprehensive performances[42]. However, the effect of sintering process on the properties of SLA nano-ZrO_2 reinforced SiO_2-based ceramic cores has not been systematically explored, and the high-temperature creep resisitance still needs furtuer exploration. In order to explore the reasonable final sintering temperature, SLA samples with varied nano-ZrO_2 contents were sintered at different final sintering temperatures. These ceramic cores were analyzed from the aspects of linear shrinkage, porosity, room/high temperature flexural strength, creep deformation, and soluble rate. An investigation on phase constitution and microstructure evolution was conducted to examine the mechanism through which the nano-ZrO_2 content and final sintering temperature exert their influence on ceramic core samples.

2 Materials and methods

2.1 Raw materials and sample preparation

The raw materials used for preparing the ceramic green bodies are listed in Table 1. Details concerning the specifications of SiO_2 and nano-ZrO_2 powders can be found in our previous work[42]. The CeraBuilder100Pro-SLA (Wuhan Intelligent Laser Technology Co., Ltd., China) was used for SLA additive manufacturing in this experiment. Different contents of nano-ZrO_2 powders, specifically 1.0wt.%, 1.5wt.%, and 2.0wt.%, were added as mineralizers to the SiO_2 powder.

The sizes of the green bodies for mechanical properties and microstructure characterization were 40 mm×5 mm×4 mm (L×W×H). The laser power was 150 mW, the scanning speed was 3, 000 mm·s^{-1}, and the layer thickness was 50 μm. The ceramic green bodies prepared through the SLA process were placed in a muffle furnace for debinding and sintering to remove the polymer resin components and obtain dense ceramic parts. The debinding stage, which involved heating the sample from room temperature to 600 °C, was executed in accordance with the sample's TG-DTG curve[42]. The heating rate during this stage was set to 0.5 °C·min^{-1}, and the process included holding at 180 °C, 275 °C, 379 °C, and 510 °C for two hours each. Beyond 600 °C, the process entered the high-temperature sintering stage. During this stage, the heating rate was increased to 2 °C·min^{-1}, and the final sintering temperatures were set at 1,150 °C, 1,200 °C, 1,250 °C, and 1,300 °C, sintered for 240 min. Figure 1 shows the details of the sintering process.

2.2 Material characterization

A digital vernier caliper was used to measure and calculate the dimensional shrinkage of the sample after sintering in the *X*, *Y*, and *Z* directions. The apparent porosity and bulk density of the sintered ceramics were determined by the Archimedean drainage method according to HB5353.1-2004. The flexural strength of the sintered ceramic was measured and calculated on the WDW-300 universal material testing machine (Changchun Kexin Experimental Instrument Co., Ltd., China) by the three-point flexural method at both room and high temperatures. The span was 30 mm, and the loading rate was 0.5 mm·min^{-1}. The sample used for testing the high-temperature flexural strength was heated to 1,550 °C at a heating rate of 5 °C·min^{-1}. The high-temperature creep resistance of the sample was measured using the double fulcrum method.

In this study, a 30% potassium hydroxide (KOH) liquid was used as the etchant. The samples for the soluble rate test were measured 10 mm×10 mm×4 mm. The main reactions occurring during the core removal process are shown in Eq. (1):

$$SiO_2 + 2KOH = K_2SiO_3 + H_2O \quad (1)$$

The specific procedure was as follows: The sintered ceramic samples were soaked in a boiled 30% KOH etching liquid. Prior to conducting the soluble rate test, the weight of the samples was measured and denoted as W_1 (g). Subsequently, batches of samples were taken out every 5 min. After rinsing thoroughly with deionized water, the samples were placed in an oven maintained at 90 °C for 120 min. Following this, the samples were weighed again to determine their weight after dissolution, denoted as W_2 (g). The weight loss percentage W (%) during the soluble rate test within the initial 30 min is computed using Eq. (2):

$$W = (W_1 - W_2)/W_1 \times 100\% \quad (2)$$

Phase analysis for the ceramic cores was performed using a D8 Advance X-ray diffractometer (XRD, Germany, Bruker AXS, Ltd.), within the 2θ range of 20° to 60° at a scanning rate of 10 °·min^{-1}. The microstructure of the ceramic cores was

Table 1: Powder materials for the ceramic cores fabricated using SLA method

Raw materials	Purity	Chemical formula	D_{50}	Mass fraction
Fused silica	99.9%	SiO_2	10.36 μm	78wt.%
Nano-zirconia	99.9%	ZrO_2	50 nm	(1–2)wt.%
Kaolin powder	–	α-Al_2O_3	7.5 μm	–

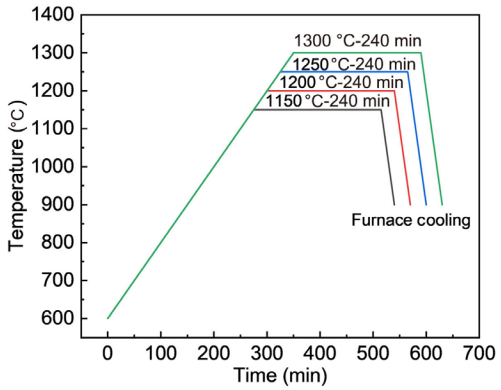

Fig. 1: Sintering process curves of SLA ceramic green bodies with different nano-ZrO_2 contents

observed by means of scanning electron microscopy (SEM, HITACHI SU 1500). The distribution of elements in the samples was analyzed using an energy dispersive spectrometer (EDS).

3 Results and discussion

3.1 Physical properties

3.1.1 Linear shrinkage

Figure 2(a) illustrates the variation in shrinkage rate of SLA SiO_2-based ceramic core samples with different final sintering temperatures and different nano-ZrO_2 contents. As the final sintering temperature increases from 1,150 °C to 1,300 °C, the shrinkage rate of ceramic core samples with the same nano-ZrO_2 content increases in the building direction. At the final sintering temperature of 1,150 °C, the SLA SiO_2-based ceramic core samples exhibit the lowest shrinkage rate. Specifically, the shrinkage rate of the SiO_2-based ceramic core sample containing 2.0wt.% nano-ZrO_2 is only 1.79% in the *Z*-direction. As the final sintering temperature increases to 1,250 °C, the shrinkage rate in the *Z*-direction of the samples containing 1.5wt.%–2.0wt.% nano-ZrO_2 rises to 3.35%–3.68%. For the same final sintering temperature, a higher nano-ZrO_2 content in the ceramic core sample results in a larger shrinkage rate in the *Z*-direction, due to the promotion of sintering and viscous flow by nano-ZrO_2. The influence of nano-ZrO_2 up to 2.0wt.% on the migration and diffusion of quartz glass, a high-temperature stable phase, can be negligible. As the final sintering temperature increases, the migration and diffusion rates of grain boundary in the SiO_2-based ceramic core sample are accelerating. During this period, the decreased viscosity of the quartz glass phase can accelerate the viscous flow. Consequently, ceramic particles gradually fill the pores left by the removed photosensitive resin, increasing the shrinkage rate.

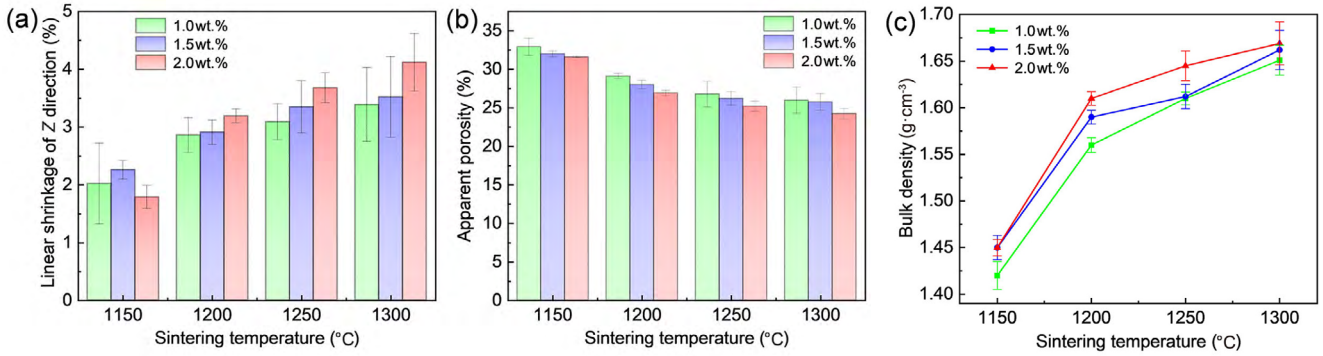

Fig. 2: Linear shrinkage (a), apparent porosity (b), and bulk density (c) of SiO_2-based ceramic core samples with different nano-ZrO_2 contents and different final sintering temperatures

3.1.2 Apparent porosity and bulk density

Figure 2(b) illustrates the changes in apparent porosity of SiO_2-based ceramic core samples with varied nano-ZrO_2 contents as the final sintering temperature is altered. As the final sintering temperature increases, the apparent porosity of the samples shows a decreasing trend, and the same trend is observed as the content of nano-ZrO_2 increases. At the final sintering temperature of 1,150 °C, the sample with 1.0wt.% nano-ZrO_2 exhibits the highest porosity of 32.91%. When the final sintering temperature rises to 1,300 °C, the porosity of the sample with the same nano-ZrO_2 content decreases to 25.97%. As the content of nano-ZrO_2 increases to 2.0wt.%, the sample sintered at 1,300 °C shows a lower porosity of 24.62%, which is lower than the sample sintered at 1,150 °C of 31.67%. At 1,250 °C, the porosity of samples, with a nano-ZrO_2 content of 1.5wt.%–2.0wt.%, ranges from 25.57% to 26.03%, both exceeding 25%, meeting the requirements for casting[43, 44].

Figure 2(c) shows the changes in bulk density of SiO_2-based ceramic core samples with different final sintering temperatures and nano-ZrO_2 contents. As the final sintering temperature increases from 1,150 °C to 1,300 °C, the bulk density of the SiO_2-based ceramic core samples gradually increases, regardless of the nano-ZrO_2 content. For the sample with 1.5wt.% nano-ZrO_2, the bulk density increases from 1.45 g·cm^{-3} to 1.66 g·cm^{-3}. Similarly, the bulk density of the sample with 2.0wt.% nano-ZrO_2 increases from 1.45 g·cm^{-3} to 1.67 g·cm^{-3}. When sintered at 1,250 °C, the bulk density ranges from 1.61 g·cm^{-3} to 1.65 g·cm^{-3} as the nano-ZrO_2 increases from 1.0wt.% to 2.0wt.%.

As shown in Figs. 2(b) and (c), with an increase in final sintering temperature, the apparent porosity decreases, while the bulk density increases. Higher final sintering temperatures can notably promote the viscous flow of the SiO_2-based ceramic cores, reducing the pore space and thereby improving the bulk density. Additionally, because the density of nano-ZrO_2 (5.58 g·cm^{-3}) is higher than that of SiO_2 (2.2 g·cm^{-3}), the addition of nano-ZrO_2 particle helps fill pores, resulting in decreased apparent porosity and increased bulk density.

3.1.3 Surface roughness

Figure 3 shows the variation of roughness on the upper and side surfaces of SLA SiO_2-based ceramic cores with different nano-ZrO_2 contents at various final sintering temperatures. As the final sintering temperature increases, the surface roughness of the SiO_2-based ceramic core samples firstly decreases and then increases. The samples sintered at a relatively lower temperature of 1,150 °C exhibit a higher surface roughness. This is attributed to the weaker adhesion between powder particles that occurs due to the lower final sintering temperature, leading

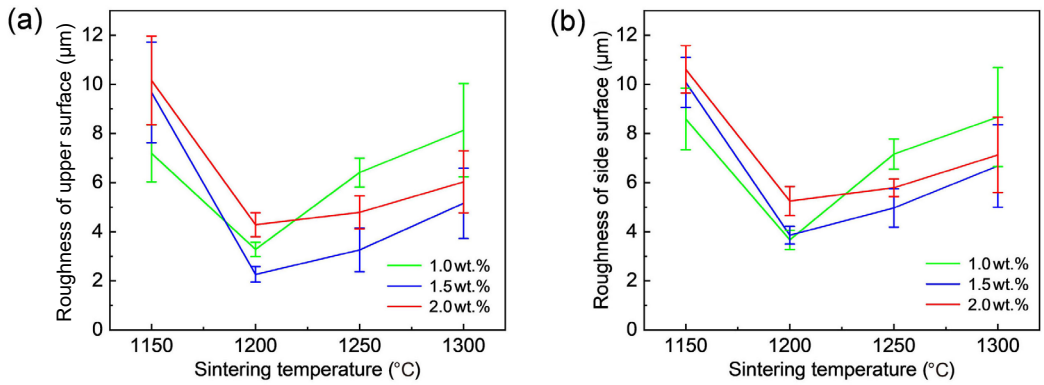

Fig. 3: Roughness of upper surface (a) and side surface (b) of SiO_2-based ceramics with different nano-ZrO_2 contents at different final sintering temperatures

to a significant loss of powder particles and consequently, a rougher surface. The surface roughness values for the upper surfaces of ceramic cores with varying nano-ZrO_2 contents are as follows: 7.19 μm for 1.0wt.%, 9.67 μm for 1.5wt.%, and 10.16 μm for 2.0wt.%. Similarly, for the side surfaces, the roughness values are 8.59 μm for 1.0wt.% nano-ZrO_2, 10.08 μm for 1.5wt.%, and 10.61 μm for 2.0wt.%. When the final sintering temperature is 1,250 °C, the upper surface roughness of the SiO_2-based ceramic core samples with different nano-ZrO_2 contents decreases to 6.41 μm, 3.26 μm, and 4.79 μm, and the side surface roughness decreases to 7.16 μm, 4.97 μm, and 5.79 μm. However, as the final sintering temperature rises to 1,300 °C, the upper surface roughness of ceramic core samples with different nano-ZrO_2 contents increases again to 8.13 μm, 5.16 μm, and 6.03 μm, and the side surface roughness increases to 8.67 μm, 6.68 μm, and 7.13 μm, respectively.

Figure 4 presents the SEM images of the upper surface morphologies of the SiO_2-based ceramic core samples after sintering at different temperatures. At the final sintering temperature of 1,150 °C, relatively complete ceramic particles are observed, exhibiting weak inter-particle bonding and minimal evidence of liquid-phase sintering. No significant defects, such as agglomeration-induced pits or particle shedding, are detected on the microstructural scale. The surface also exhibits a few cracks formed by the connection of continuous pores. As the final sintering temperature increases to 1,250 °C, the surface temperature of the sample becomes higher than the internal temperature. An increase in the liquid phase can be observed on the surface of the ceramic core samples. Since the buried sintering is carried out within the Kaolin α-Al_2O_3 powders, the liquefied ceramic particles on the surface remain relatively flat after sintering. The pores on the surface of the core samples are significantly reduced by liquid phase flow refusion. Additionally, the cristobalite precipitated from the quartz glass can cause surface cracks due to volume shrinkage during cooling. Furthermore, more cristobalite precipitates due to the high final sintering temperature of 1,300 °C. It results in the growth of more “hill-like” protrusions with pointed tips on the surface

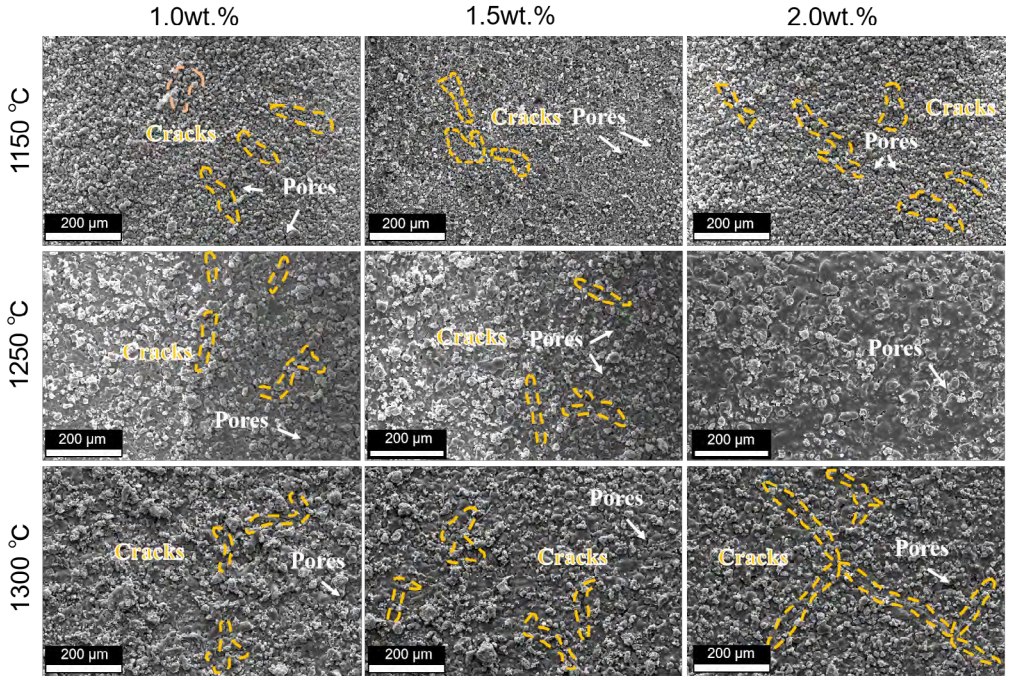

Fig. 4: SEM images showing the upper surface morphologies of SiO_2-based ceramics with different nano-ZrO_2 contents at different final sintering temperatures

of liquid phase, which are more obvious than the sample sintered at 1,250 °C, leading to increased surface roughness. Figure 5 shows the SEM images of the side surface roughness of the SiO_2-based ceramic core samples. At all final sintering temperatures, the side surface remains relatively flat without significant delamination or fractures. As the final sintering temperature increases to 1,250 °C and 1,300 °C, the surface ceramic particles also merge into the liquid phase, making it difficult to observe the interlayer structure.

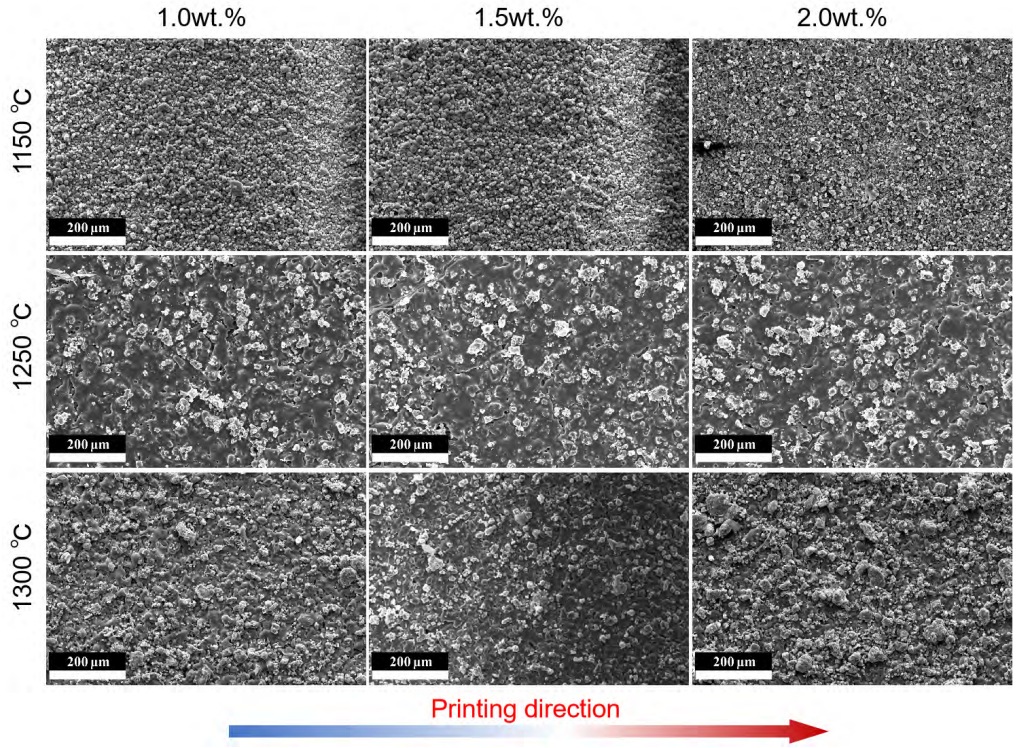

Fig. 5: SEM images showing the side surface morphologies of SiO_2-based ceramics with different nano-ZrO_2 contents at different final sintering temperatures

3.2 Mechanical properties

3.2.1 Room-temperature flexural strength

Figure 6 shows the room-temperature flexural strength of SiO_2-based ceramic core samples with varied nano-ZrO_2 contents at different final sintering temperatures. With an increase in final sintering temperature, the room-temperature flexural strength initially increases and then slightly decreases. When the final sintering temperature is 1,150 °C, the room temperature flexural strengths of the samples are 7.58 MPa for 1.0wt.% nano-ZrO_2, 7.51 MPa for 1.5wt.%, and 8.1 MPa for 2.0wt.%, which are difficult to meet the basic strength requirements for ceramic cores[45]. As the final sintering temperature increases to 1,250 °C, the room temperature flexural strength of samples reaches its maximum values of 24.11 MPa for 1.0wt.% nano-ZrO_2, 26.79 MPa for 1.5wt.%, and 27.85 MPa for 2.0wt.%. For the SiO_2-based ceramic cores with 1.0wt.%–2.0wt.% nano-ZrO_2 contents, the average room temperature flexural strength of the sample sintered at 1,250 °C is 9.34 % higher than that of the sample sintered at 1,200 °C.

The increase in the final sintering temperature and the resultant increasing viscous flow of the quartz glass can improve the densification of ceramic cores and thus increase their strength. In addition, the room-temperature flexural strength of SiO_2-based ceramic cores is mainly affected by the transformation of quartz glass phase into cristobalite. Figure 7 shows the XRD patterns of samples with different nano-ZrO_2 contents at different final sintering temperatures. The ceramic core sample sintered at 1,150 °C has a lower quartz content (less than 2.83%). In the study on the kinetics and mechanical performance of refractory fused silica, Bae et al.[46] concluded that there was only a small amount of cristobalite precipitates below 1,200 °C, and the amount of cristobalite was even lower when sintering at 1,150 °C. Therefore, the enhancement of room temperature strength by cristobalite at this temperature is limited. As can be seen in Fig. 7(d), with an increase in final

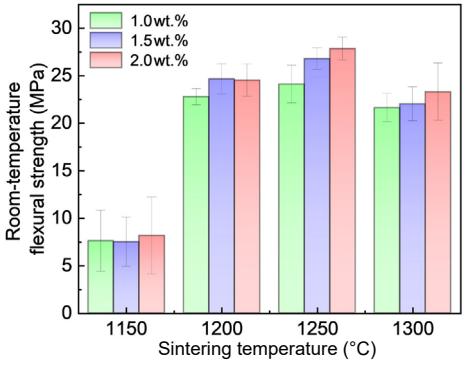

Fig. 6: Room temperature flexural strength of SiO_2-based ceramics with varied nano-ZrO_2 contents at different final sintering temperatures

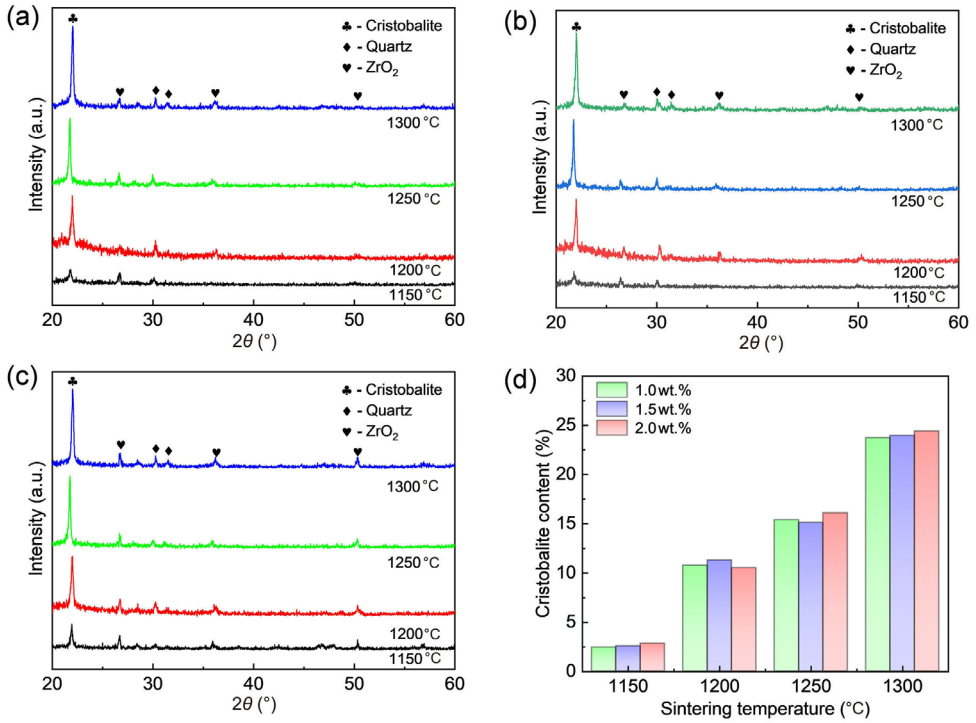

Fig. 7: XRD patterns of SiO_2-based ceramics with varied nano-ZrO_2 contents at different final sintering temperatures: (a) 1.0wt.%; (b) 1.5wt.%; (c) 2.0wt.%; and (d) cristobalite contents

sintering temperature, the precipitation amounts of cristobalite in the SiO_2-based ceramic core samples gradually increases. Due to the low content of ZrO_2, there is no obvious difference in the content of cristobalite in the ceramic core samples sintered at the same temperature. When the final sintering temperature rises to 1,250 °C, the average quartz content in the SiO_2-based ceramic cores with various nano-ZrO_2 contents is 15.54%. When the temperature reaches 1,300 °C, the precipitation of cristobalite in the ceramic samples increases significantly, with its average content reaching 24.04%. Consequently, at this stage, the enhanced strength of sintered particles and the formation of cristobalite play a dominant role in microstructural development. Excessive generation of cristobalite will be accompanied by volume expansion, causing damage to the stable structure of the surrounding particles. It can increase the internal stress and even damaging the grain morphology, which is also the reason why the flexural strength of the ceramic core samples firstly increases and then decreases.

Figures 8 and 9 show the fracture morphology and EDS surface mapping of SiO_2-based ceramic core samples with varied nano-ZrO_2 contents, which have undergone sintering at different temperatures and subsequent flexural testing at room temperature. It can be seen that the interior of the ceramic cores is mainly composed of large ceramic particles as the skeleton, with small ceramic particles filling the pores or attaching the large particles. Additionally, in samples with the same nano-ZrO_2 content but different final sintering temperatures, the higher the final sintering temperature, the more uniform the distribution of nano-ZrO_2. It can be observed from Fig. 8 that, at a sintering temperature of 1,150 °C, the fracture morphologies of the three groups of ceramic core samples reveal loose bonding between SiO_2 particles. There are numerous pores present within the spherical SiO_2 powder, and the particle shape remains relatively uniform across the samples. As the final sintering temperature increases to 1,250 °C, the bonding between the ceramic particles is tighter, the number of pores decreases significantly, and the room-temperature mechanical properties are improved by a better sintering effect. At this time, the shape of the ceramic particles still remains relatively complete and spherical. When the final sintering temperature further increases to 1,300 °C, a higher fraction of liquid phase can be observed, and the growth of grains and the movement of grain boundaries are more obvious. The micro-cracks on the surface of ceramic particles can be observed, which are mainly due to an increase in the precipitation of cristobalite resulted by the higher final sintering temperatures. At the same time, because the nucleation of cristobalite is heterogeneous, it firstly forms on the surface of quartz glass and then gradually expands to the interior of quartz glass. Therefore, cracks caused by the volume change due to the transformation of α-cristobalite to β-cristobalite also increase. The ocurrence of micro-cracks will of course deteriorate the room-temperature mechanical properties of core samples.

3.2.2 High-temperature flexural strength

Figure 10 illustrates the high-temperature flexural strength, measured at 1,550 °C, of SiO_2-based ceramic core samples that contain differing amounts of nano-ZrO_2 and have been sintered at various temperatures. It can be noted that the high-temperature flexural strength test essentially simulates a secondary sintering

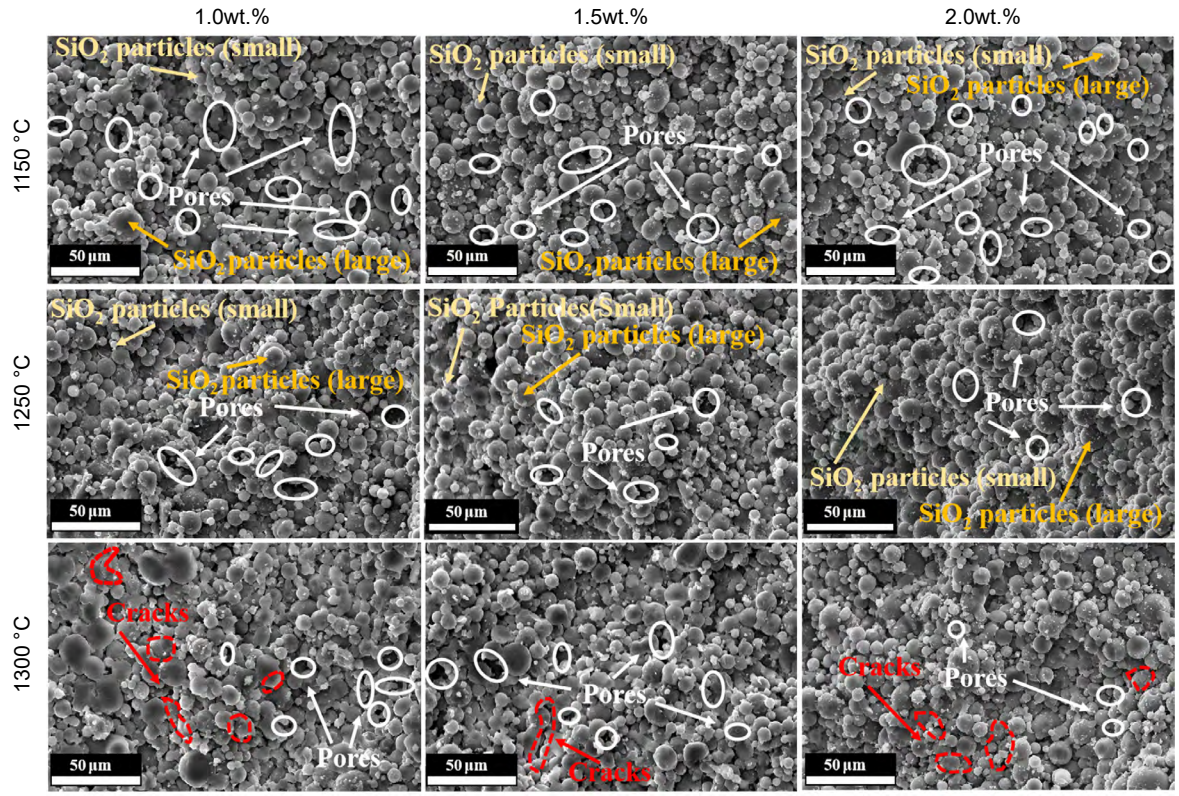

Fig. 8: SEM images of SiO_2-based ceramics with varied nano-ZrO_2 contents at different final sintering temperatures after room temperature flexural testing

process, conducted at 1,550 °C for 30 min. The observed variation of the flexural strength at high temperatures is consistent with that at room temperature, both showing a trend of initially increase and then decrease with an increase in the final sintering temperature. At the final sintering temperature of 1,250 °C, the high-temperature flexural strength of the SiO_2-based ceramic core samples with different nano-ZrO_2 contents reaches the maximum values, which are 27.77 MPa for 1.0wt.% nano-ZrO_2, 30.77 MPa for 1.5wt.%, and 33.02 MPa for 2.0wt.%. As the final sintering temperature further increases to 1,300 °C, the high-temperature strength of the core samples with different nano-ZrO_2 contents decreases to 25.79 MPa, 24.87 MPa, and 24.21 MPa, respectively.

Figure 11 shows the fracture surfaces of the ceramic core samples after a high-temperature flexural strength test, conducted after holding at 1,550 °C for 30 min. It can be seen that the fracture surfaces of all the SiO_2-based ceramic core samples exhibit a relatively smooth appearance, with the majority of fractures occurring in a transgranular mode. Transgranular fracture requires more energy, indicating that the material possesses superior flexural performance. In addition, cracks can be observed on the fracture surfaces. For ceramic core samples sintered at the same final sintering temperature, the size of cracks gradually decreases with the increase of nano-ZrO_2 content. In the ceramic core samples with the same nano-ZrO_2 content, the number of cracks on the high-temperature fracture surface is the lowest when sintered at a final temperature of 1,250 °C. This correlates with its superior performance in high-temperature flexural strength.

XRD phase analysis was performed on the samples after the high-temperature flexural strength test, and their phase constitutions are shown in Figs. 12(a) to (c). The diffraction peaks in the XRD patterns are similar, with the main difference being the $ZrSiO_4$ diffraction peak formed by SiO_2 and ZrO_2 in the 1550 °C high temperature conditions. The height of these peaks is positively correlated with the addition amount of nano-ZrO_2. From Figs. 12(a) to (c), it can be seen that after the ceramic core samples are held at 1,550 °C for 30 min, the peak value of the cristobalite diffraction around 22° in the XRD phase diagram increases. Figure 12(d) indicates the variation of cristobalite content in the samples with different nano-ZrO_2 contents that sintered at different final sintering temperatures and then being held at 1,550 °C for 30 min. After the equivalent secondary sintering during the high-temperature flexural strength test, the average quartz content of the samples, which underwent various final sintering temperatures, is found to be 34.8%, 35.84%, 36.33%, and 37.23%, respectively. Following the equivalent secondary sintering, the samples with higher final sintering temperatures during the first sintering have a slightly higher quartz content. This is mainly due to the reason that more cristobalite is generated during the first sintering, which can promote the precipitation of cristobalite during the secondary sintering. Zhang[47] and Wang[48] suggested that $ZrSiO_4$ acted as a heterogeneous nucleation agent, promoting the precipitation of cristobalite. However, in Fig. 12(d), there is no significant difference in quartz content after secondary sintering. Wilson[49] argued that $ZrSiO_4$ had no effect on quartz precipitation in SiO_2-based ceramic cores. Considering the minimal amount of $ZrSiO_4$ generated at high temperatures in this experiment, it can be concluded that $ZrSiO_4$ had no influence on precipitation of quartz.

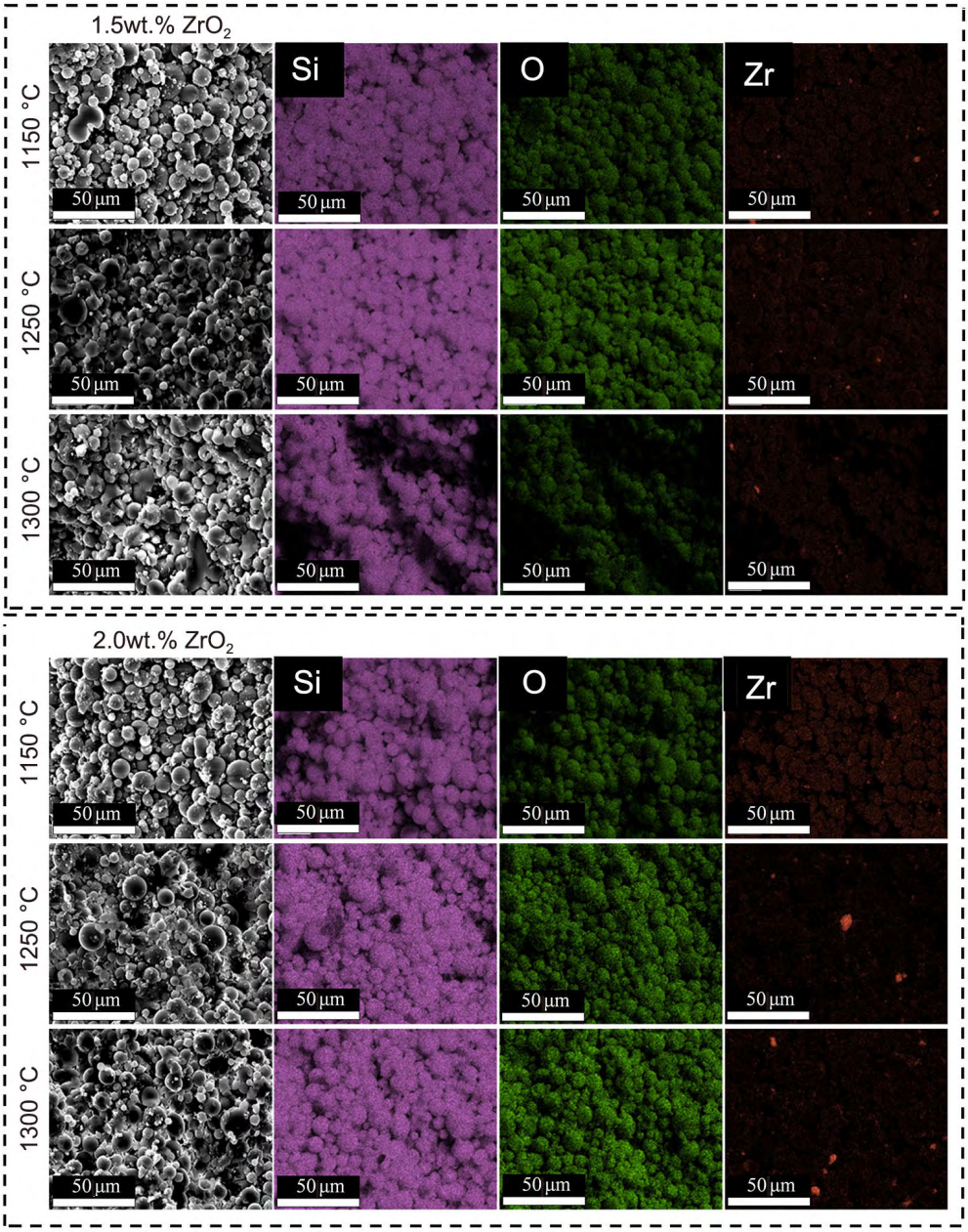

Fig. 9: EDS surface mappings of Si, O, and Zr element distribution of SiO_2-based ceramics with varied nano-ZrO_2 contents at different final sintering temperatures

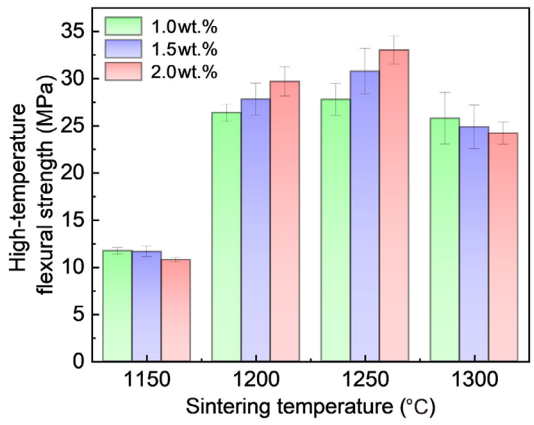

Fig. 10: High-temperature flexural strength of SiO_2-based ceramics with different nano-ZrO_2 contents at different final sintering temperatures

3.2.3 High-temperature creep resistance

The high-temperature creep resistance of the ceramic cores is primarily caused by the viscous flow of quartz glass at high temperatures. When the cristobalite content in the ceramic cores is insufficient before casting, it resulting in poor creep resistance of the cores, making it prone to softening and deformation when surrounded by molten metal[50]. Figure 13 shows the high-temperature deflection data of ceramic core samples with different nano-ZrO_2 contents at various final sintering temperatures. As the final sintering temperature increases, the high-temperature deflection of the ceramic cores gradually decreases. When the final sintering temperature exceeds 1,250 °C, the decrease in high-temperature creep deformation becomes less pronounced. At the final sintering temperature of 1,250 °C, the high-temperature deflection of the ceramic samples with different nano-ZrO_2 contents is 7.99 mm,

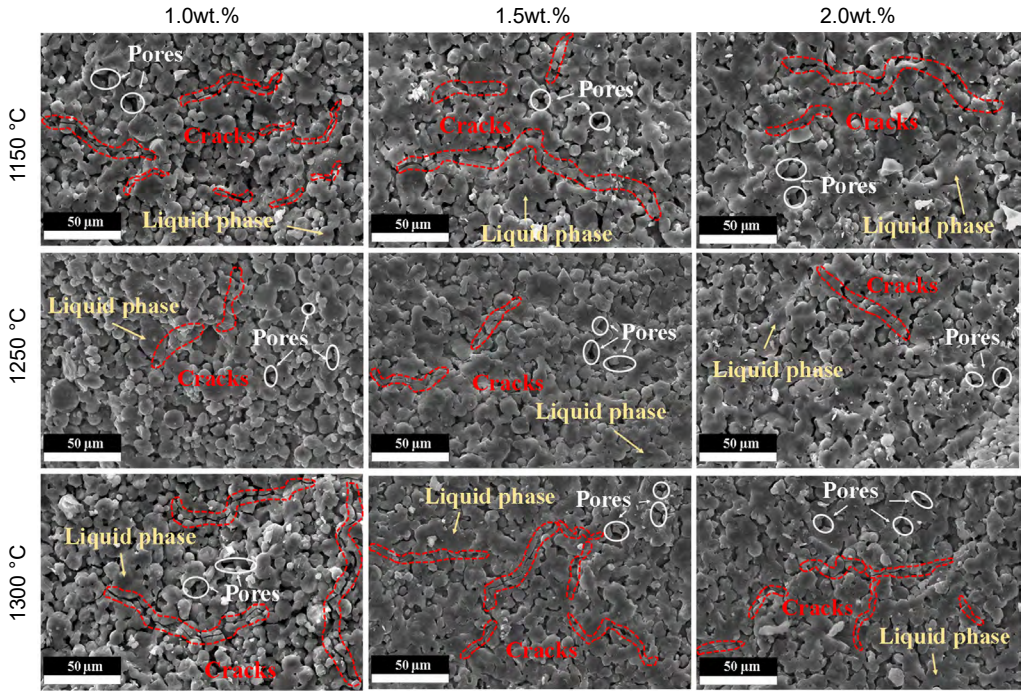

Fig. 11: SEM images of SiO_2-based ceramics with different nano-ZrO_2 contents at different final sintering temperatures after high-temperature flexural testing

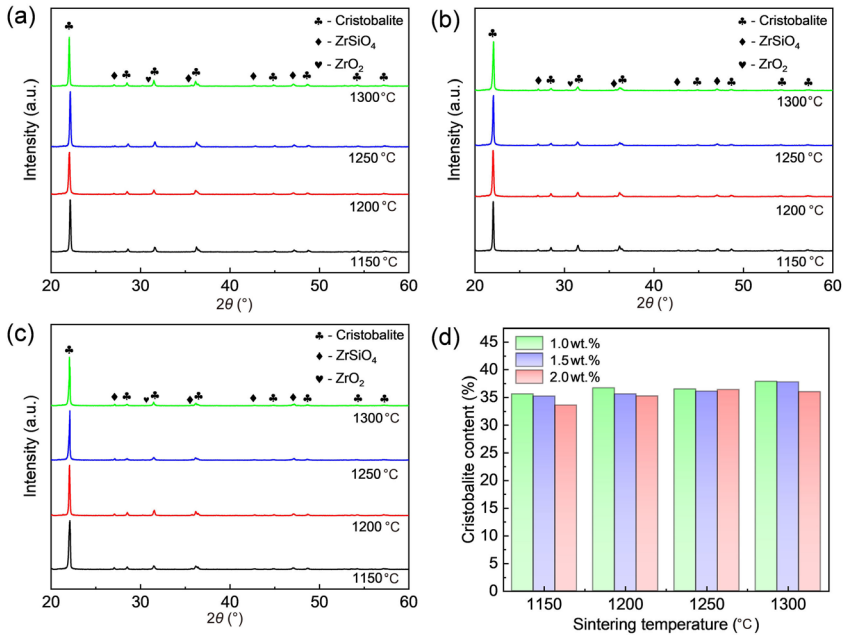

Fig. 12: XRD patterns of SiO_2-based ceramics with different nano-ZrO_2 contents at different final sintering temperatures after high-temperature flexural testing: (a) 1.0wt.%; (b) 1.5wt.%; (c) 2.0wt.%; and (d) variation of cristobalite content

5.31 mm, and 3.37 mm, respectively. Compared to the samples sintered at 1,200 °C, their high-temperature deflection of samples with different nano-ZrO_2 contents decreases by 54.05%, 66.11%, and 62.34%, respectively. When the final sintering temperature further increases to 1,300 °C, the high-temperature deflection of the core samples with different nano-ZrO_2 contents further reduces to 7.23 mm, 5.01 mm, and 3.21 mm, respectively.

In the analysis of the variation in cristobalite content within the ceramic core that underwent secondary sintering at 1,550 °C, as depicted in Fig. 12(d), a notable increase in cristobalite content is observed when compared to the first sintering process [Fig. 7(d)], as indicated by the increased area of the diffraction peaks. In high-temperature environments, cristobalite, as a high-temperature stable reinforcing phase, can improve the high-temperature creep resistance of ceramic core samples. The high-temperature deflection of the ceramic core samples in Fig. 13 varies significantly with the final sintering temperature. This is mainly because the high-temperature creep of the SiO_2-based ceramic core samples is not only related to the content of cristobalite formed during the holding period at 1,550 °C, but also the transformation rate of cristobalite during

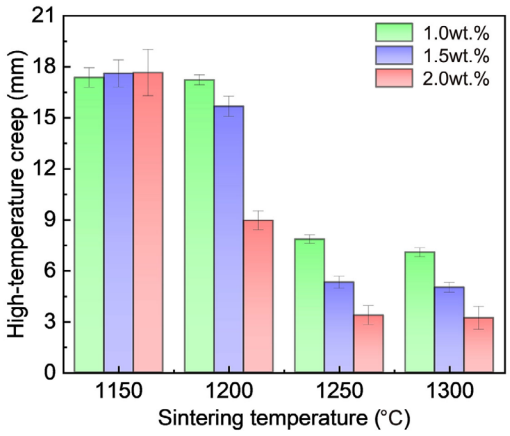

Fig. 13: High-temperature creep and deflection of SiO_2-based ceramics with various nano-ZrO_2 contents at different sintering temperatures

the sintering process. During the first sintering process, as the final sintering temperature increases, the content of cristobalite in the SiO_2-based ceramic core samples also increases. During the secondary sintering, the cristobalite content is higher, thus enabling the ceramic cores to achieve enhanced high-temperature creep resistance more quickly. In addition, $ZrSiO_4$, formed from the reaction between ZrO_2 and SiO_2 at high-temperatures, can also act as a high-temperature stable substance to prevent the creep of quartz glass [39].

Figures 14 and 15 show the fracture surface morphology and the corresponding EDS surface mapping of the ceramic core samples after high-temperature creep testing, respectively. The microstructural evolutions of the ceramic core after high-temperature holding can be observed. It can be seen that after holding at 1,550 °C, the ceramic particles become denser and significantly passivated. Furthermore, it is difficult to observe complete spherical ceramic particles, which is mainly due to the presence of a liquid phase. The liquid phase flows more frequently under the action of capillary force, which can further enhance the density and improve the mechanical properties of the samples at high temperatures. Due to the volume effects of cristobalite during the cooling process, a large number of cracks are observed in the samples after high-temperature treatment at 1,550 °C. As shown in Fig. 15, the Zr element primarily exists in the forms of ZrO_2 and $ZrSiO_4$, and is distributed across the surface of SiO_2 grains. In this context, $ZrSiO_4$ functions as a reinforcing network that effectively hinders the viscous flow of the glass phase at high temperatures, subsequently mitigating high-temperature creep deformation.

3.3 Soluble rate

Figure 16 shows the soluble rate of the ceramic samples with different final sintering temperatures and different nano-ZrO_2 contents. The SiO_2-based ceramic core samples sintered at 1,150 °C have a relatively rapid soluble rate. Due to their insufficient sintering, the corrosive liquid quickly destroys the bonding force between particles, causing the samples to dissolve into separate small blocks within 5 min. This increases the contact area between the samples and the corrosive liquid, resulting in a weight loss rate of 55%, 50%, and 49%, respectively within 10 min of the start of soluble rate test. In addition, all ceramic core samples are dissolved within 20 min. At final sintering temperatures of 1,250 °C and 1,300 °C, a liquid phase envelops the surface of the core samples, resulting in a reduced number of pores. Consequently, the corrosive liquid encounters initial resistance in permeating the core, thereby slowing down the dissolution rate. After 10 min,

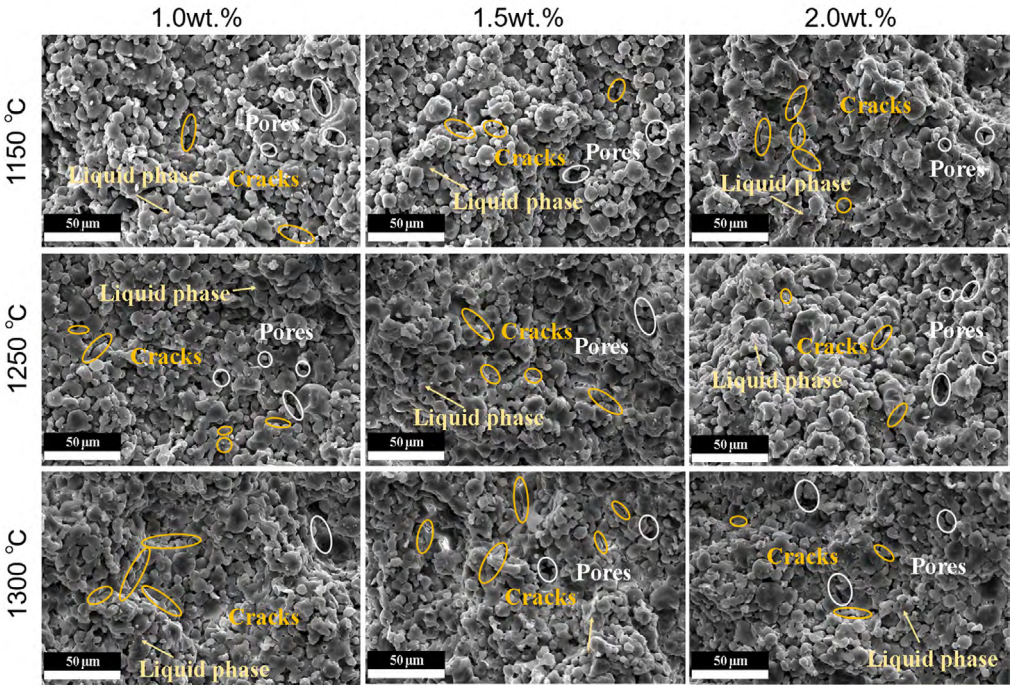

Fig. 14: SEM images of SiO_2-based ceramics with different nano-ZrO_2 contents sintered at different final sintering temperatures after high-temperature deflection test

the weight loss rates of samples sintered at 1,250 °C with different nano-ZrO_2 contents are 15%, 16%, and 12%, while those sintered at 1,300 °C are 12%, 13%, and 11%, respectively. Under all final sintering temperatures and varying nano-ZrO_2 contents, the core samples are completely dissolved within 30 min, meeting the requirements for shell removal of investment casting process[44].

3.4 Influence mechanism of final sintering temperature

Figure 17 illustrates the influence of sintering temperature changes on SiO_2-based ceramic cores with varied contents of nano-ZrO_2. The matrix material is composed of spherical SiO_2 powder. When the ceramic core is sintered at 1,150 °C, the relatively low sintering conditions lead to bonding predominantly through point-contact interactions among the particles. Consequently, the matrix ceramic particles predominantly maintain their fully spherical morphology. Quartz glass precipitates less at a lower temperature, providing insufficient strength enhancement to the samples[46]. When sintered at 1,250 °C, the ceramic core undergoes significant microstructural evolution as interparticle bonding transitions from discrete point contacts to continuous surface interfaces. The higher temperature increases the occurrence frequency

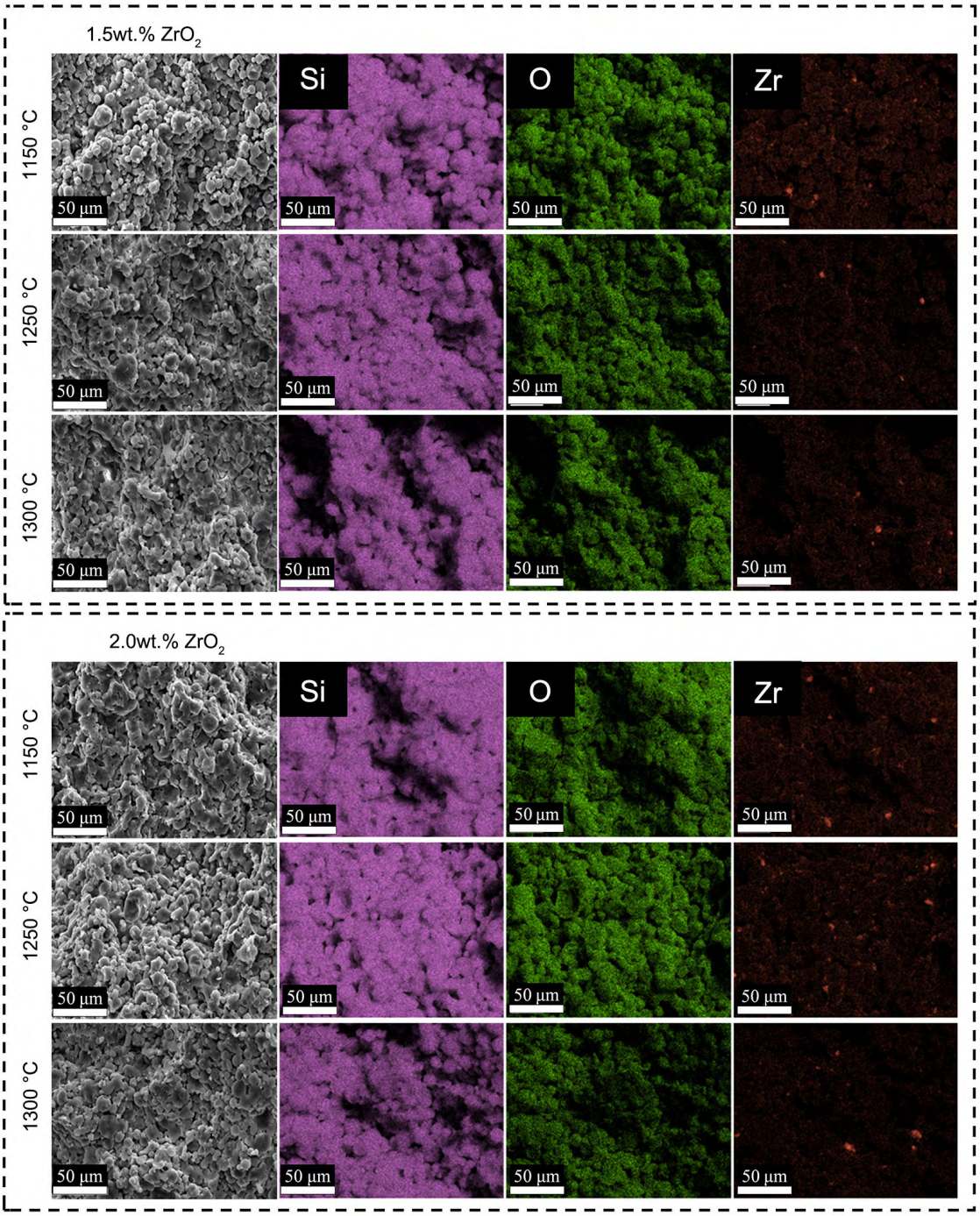

Fig. 15: EDS images showing surface mappings of Si, O, and Zr elements of SiO_2-based ceramic cores with different nano-ZrO_2 contents at different final sintering temperatures after high-temperature creep test

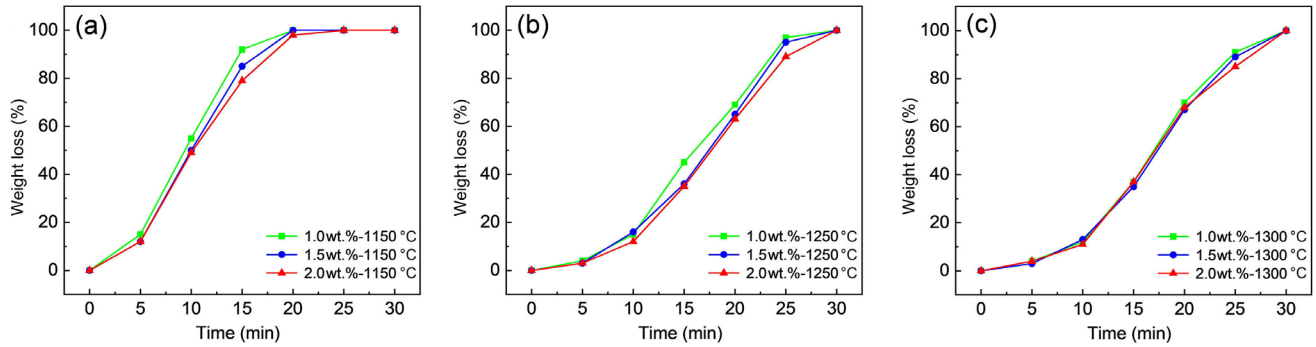

Fig. 16: Dissolution rate of SiO_2-based ceramics with different nano-ZrO_2 contents and different final sintering temperatures: (a) 1,150 °C; (b) 1,250 °C; (c) 1,300 °C

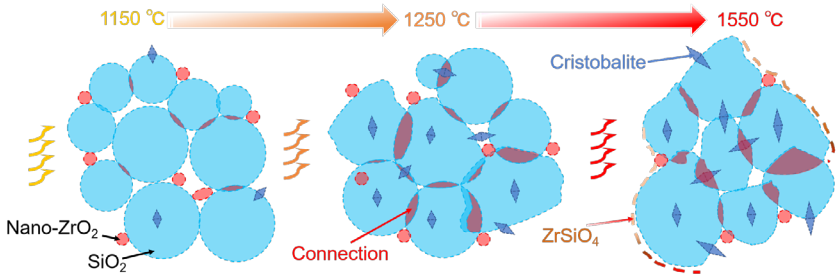

Fig. 17: Schematic diagram of SiO_2-based ceramics with different final sintering temperatures

of viscous flow, which gradually eliminates large pores and accelerates the shrinkage rate of the ceramic core samples. Moreover, the elevated final sintering temperature promotes the crystallization of quartz glass. It initially forms on the surface of the matrix particles and gradually grows into the interior of the matrix particles. As the temperature increases, both the rate and quantity of cristobalite precipitated from quartz glass also increase. An appropriate amount of cristobalite can provide stable support within the core, enhancing its mechanical properties. However, during the cooling process, cristobalite undergoes a volume shrinkage of approximately 2.8%[51], which can create cracks within the core, thereby reducing its room temperature strength. The added nano-ZrO_2 in the core, being a neutral ion and present in small amounts, does not significantly affect on the precipitation of cristobalite. In summary, after a single sintering process, both the sintering-promoting effect of nano-ZrO_2 and the intensified viscous flow at elevated temperatures elevate the sintering degree of the cores, leading to increased shrinkage of core samples, reduced apparent porosity, and increased bulk density. Additionally, denser sintering and the increase in cristobalite content contribute to improved mechanical properties at room temperature. However, samples sintered at 1,300 °C are more susceptible to the volume shrinkage of cristobalite, resulting in cracks and consequently leads to a deterioration in room temperature mechanical properties.

For SiO_2-based ceramic cores, quartz glass undergoes viscous flow at high temperatures, leading to softening and deformation of the cores. During sintering, cristobalite precipitates from the ceramic cores. Cristobalite, characterized by its robust covalent bonds, maintains thermodynamic stability within a temperature range of 1,470–1,728 °C[52], showcasing remarkable high-temperature stability. Cristobalite exhibits minimal high-temperature creep and avoids experiencing viscous flow, in contrast to amorphous quartz glass. Therefore, cristobalite can act as a high-temperature stable phase in a SiO_2-based core, inhibiting liquid-phase viscous flow. Additionally, it can form an interlocking structure with quartz glass, further enhancing the high-temperature creep resistance of the cores. Although the cristobalite content in the ceramic core samples obtained at various final sintering temperatures is similar after holding at 1,550 °C for 30 min, a higher final sintering temperature during the initial sintering allows the core to have more cristobalite. After the first sintering, the cristobalite within the cores can serve as nucleation sites for cristobalite transformation during the secondary sintering, promoting the conversion of quartz glass into cristobalite crystals. This early formed cristobalite provides the cores with excellent creep resistance at an earlier stage. Additionally, because the added nano-ZrO_2 is primarily distributed on the surface of the matrix ceramic particles, it more readily reacts with the liquid phase on the particle surface at high temperatures to form $ZrSiO_4$. The generated $ZrSiO_4$ can connect each other on the liquid surface to form a network structure, further inhibiting high-temperature creep deformation. Overall, the precipitation of cristobalite and the formation of $ZrSiO_4$ significantly inhibit high-temperature creep deformatiom.

4 Conclusions

This study discussed the effects of varying nano-ZrO_2 contents (1.0wt.%, 1.5wt.%, 2.0wt.%) in photocurable SiO_2-based ceramic cores on their physical properties, mechanical

properties, and surface quality at different final sintering temperatures (1,150 °C, 1,250 °C, 1,300 °C). The study also examined the underlying mechanisms through an analysis of phase constitution and microstructure evolutions. The main conclusions are as follows:

(1) As the final sintering temperature increases from 1,150 °C to 1,300 °C, both the shrinkage rate and bulk density of the photocurable SiO_2-based ceramic core samples gradually increase, while the porosity decreases. The room-temperature and high-temperature flexural strengths firstly increase and then decreases, and the high-temperature deflection gradually decreases. The surface roughness of both the upper surfaces and side surfaces initially decreases and then increases. Sufficient porosity allows the core samples to completely dissolve within 30 min.

(2) Increasing the final sintering temperature and adding nano-ZrO_2 enhance the viscous flow of quartz glass during sintering, resulting in tighter particle bonding and improved sintering degree. SiO_2-based ceramic cores sintered at 1,250 °C exhibit a higher amount of cristobalite and optimal mechanical properties at room temperature. However, when the final sintering temperature reaches 1,300 °C, the structural damage to the core material becomes more pronounced, leading to a degradation of mechanical properties and an increase in surface roughness. This is attributed to the substantial precipitation of cristobalite on the surface.

(3) Increasing the final sintering temperature allows for more cristobalite to precipitate in SiO_2-based ceramic cores after the first sintering. This can enhance the rate of transformation from the amorphous quartz glass to cristobalite during the secondary sintering, effectively inhibiting the viscous flow of quartz glass and improving the high-temperature strength and resistance to high-temperature creep of the core samples. At 1,550 °C, nano-ZrO_2 reacts with SiO_2 to form an enhanced $ZrSiO_4$ network. This network, in conjunction with cristobalite, helps to further inhibit viscous flow and reduce high-temperature deflection.

Acknowledgments

This work was supported by the Natural Science Foundation of Shanghai (No. 23ZR1421500), the National Natural Science Foundation of China (Nos. 52474412, 52127807, 52271035), the Shanghai Municipal Commission of Economy and Informatization (No. GYOJ2022-2-02), the United Innovation Program of Shanghai Commercial Aircraft Engine (No. AR966), the SPMI Project from Shanghai Academy of Spaceflight Technology (No. SPMI2022-06), and the Ningbo International Science and Technology Cooperation Program (No. 2023H004).

Conflict of interest

The authors declare that they have no known competing financial interests or personal relationships that could have appeared to influence the work reported in this paper.

References

[1] Tang W, Zhao T, Dou R, et al. Additive manufacturing of low-shrinkage alumina cores for single-crystal nickel-based superalloy turbine blade casting. Ceramics International, 2022, 48(11): 15218–15226.
[2] Gudivada G, Pandey A K. Recent developments in nickel-based superalloys for gas turbine applications: Review. Journal of Alloys and Compounds, 2023, 963: 171128.
[3] Li X T, Ma Q S, Liu E, et al. Order phase transition of HIP nickel-based powder superalloy during isothermal aging. Journal of Alloys and Compounds, 2025, 1010: 177269.
[4] Wright L M, Han J C. Heat transfer enhancement for turbine blade internal cooling. The American Society of Mechanical Engineers, 2014, 21(2–3): 111–140.
[5] Wilcock R C, Young J B, Horlock J H. The effect of turbine blade cooling on the cycle efficiency of gas turbine power cycles. Journal of Engineering for Gas Turbines and Power, 2005, 127(1): 109–120.
[6] Kanyo J E, Schafföner S, Uwanyuze R S, et al. An overview of ceramic molds for investment casting of nickel superalloys. Journal of the European Ceramic Society, 2020, 40(15): 4955–4973.
[7] Wang F, Liu Y, Yang Q, et al. Microscale stray grains formation in single-crystal turbine blades of Ni-based superalloys. Journal of Materials Science & Technology, 2024, 191: 134–145.
[8] Li J G, An X L, Liang J J, et al. Recent advances in the stereolithographic three-dimensional printing of ceramic cores: Challenges and prospects. Journal of Materials Science & Technology, 2022, 117: 79–98.
[9] Wang W Q, Zhang L, Dong X J, et al. Additive manufacturing of fiber reinforced ceramic matrix composites: Advances, challenges, and prospects. Ceramics International, 2022, 48(14): 19542–19556.
[10] Subramanian K, Vail N, Barlow J, et al. Selective laser sintering of alumina with polymer binders. Rapid Prototyping Journal, 1995, 1(2): 24–35.
[11] Wang X G, Zhou Y L, Zhou L, et al. Microstructure and properties evolution of silicon-based ceramic cores fabricated by 3D printing with stair-stepping effect control. Journal of the European Ceramic Society, 2021, 41(8): 4650–4657.
[12] Xu W L, Lu Z L, Tian G Q, et al. Fabrication of single-crystal superalloy hollow blade based on integral ceramic mold. Journal of Materials Processing Technology, 2019, 271: 615–622.
[13] Li Q L, Chen T C, Liang J J, et al. Manufacturing of ceramic cores: From hot injection to 3D printing. Journal of Materials Science & Technology, 2023, 134: 95–105.
[14] Zheng W, Wu J M, Chen S, et al. Preparation of high-performance silica-based ceramic cores with B_4C addition using selective laser sintering and SiO_2-Al_2O_3 sol infiltration. Ceramics International, 2023, 49(4): 6620–6629.
[15] Nazari K, Tran P, Tan P, et al. Advanced manufacturing methods for ceramic and bioinspired ceramic composites: A review. Open Ceramics, 2023, 15: 100399.
[16] Diao Q, Zeng Y, Chen J M. The applications and latest progress of ceramic 3D printing. Additive Manufacturing Frontiers, 2024, 3(1): 200113.
[17] Zheng W, Wu J M, Chen S, et al. Fabrication of high-performance silica-based ceramic cores through selective laser sintering combined with vacuum infiltration. Additive Manufacturing, 2021, 48: 102396.
[18] Dong Y, Jiang H, Chen A, et al. Near-zero-shrinkage Al_2O_3 ceramic foams with coral-like and hollow-sphere structures via selective laser sintering and reaction bonding. Journal of the European Ceramic Society, 2021, 41(16): 239–246.

[19] Liu K, Sun H Y, Shi Y S, et al. Research on selective laser sintering of Kaolin-epoxy resin ceramic powders combined with cold isostatic pressing and sintering. Ceramics International, 2016, 42(9): 10711–10718.
[20] Wang K J, Yang G J, Liu R Z. High-temperature ablation performance of Si_3N_4-Si_2N_2O-BN composites prepared using selective laser sintering. Corrosion Science, 2022, 204: 110404.
[21] Wu H H, Li D C, Tang Y P, et al. Rapid fabrication of alumina-based ceramic cores for gas turbine blades by stereolithography and gelcasting. Journal of Materials Processing Technology, 2009, 209(18–19): 5886–5891.
[22] Zhao G, Hu K H, Feng Q, et al. Creep mechanism of zircon-added silica ceramic cores formed by stereolithography. Ceramics International, 2021, 47(12): 17719–17725.
[23] Johansson E, Lidström O, Johansson J, et al. Influence of resin composition on the defect formation in alumina manufactured by stereolithography. Materials, 2017, 10(2): 138.
[24] Li X, Su H J, Dong D, et al. In-situ $Y_3Al_5O_{12}$ enhances comprehensive properties of alumina-based ceramic cores by vat photopolymerization 3D printing. Additive Manufacturing, 2023, 73: 103645.
[25] Yang K, Li Q L, Chen T C, et al. High-performance 3D-printed Al_2O_3 cores for low-temperature sintering. Ceramics International, 2023, 49(22, Part B): 36894–36906.
[26] Li H, Liu Y S, Colombo P, et al. The influence of sintering procedure and porosity on the properties of 3D printed alumina ceramic cores. Ceramics International, 2021, 47(19): 27668–27676.
[27] Li X, Liu Z P, Niu S X, et al. Controlled anisotropy in 3D printing of silica-based ceramic cores through oxidization reaction of aluminum powders. Ceramics International, 2023, 49(15): 24861–24867.
[28] Li Q L, An X L, Liang J J, et al. Balancing flexural strength and porosity in DLP-3D printing Al_2O_3 cores for hollow turbine blades. Journal of Materials Science & Technology, 2022, 104: 19–32.
[29] Komissarenko D A, Sokolov P S, Evstigneeva A D, et al. Rheological and curing behavior of acrylate-based suspensions for the DLP 3D printing of complex zirconia parts. Materials, 2018, 11(12). http://doi.org/10.3390/ma11122350
[30] Shi Y S, Yan C Z, Song B, et al. Recent advances in additive manufacturing technology: Achievements of the rapid manufacturing center in huazhong university of science and technology. Additive Manufacturing Frontiers, 2024, 3(2): 200144.
[31] Chen H D, Pan Y Y, Chen B, et al. Fabrication of porous aluminum ceramics beyond device resolution via stereolithography 3D printing. Ceramics International, 2023, 49(11, Part B): 18463–18469.
[32] Zheng W, Wu J M, Chen S, et al. Improved mechanical properties of SiC fiber reinforced silica-based ceramic cores fabricated by stereolithography. Journal of Materials Science & Technology, 2022, 116: 161–168.
[33] Sun J, Binner J, Bai J. Effect of surface treatment on the dispersion of nano zirconia particles in non-aqueous suspensions for stereolithography. Journal of the European Ceramic Society, 2019, 39(4): 1660–1667.
[34] Pamu D, Lakshmi N R G, James R K C, et al. Enhanced microwave dielectric properties of $(Zr0.8,Sn0.2)TiO_4$ ceramics with the addition of its own nanoparticles. Journal of the American Ceramic Society, 2011, 95(1): 126–132.
[35] Mu Y H, Chen J W, An X L, et al. Effect of synergism of solid loading and sintering temperature on microstructural evolution and mechanical properties of 60 vol% high solid loading ceramic core obtained through stereolithography 3D printing. Journal of the European Ceramic Society, 2023, 43(2): 661–675.
[36] Qian C C, Hu K H, Shen Z, et al. Effect of sintering aids on mechanical properties and microstructure of alumina ceramic via stereolithography. Ceramics International, 2023, 49(11, Part A): 17506–17523.
[37] Yang Q H, Zeng Z J, Xu J, et al. Effect of La_2O_3 on microstructure and transmittance of transparent alumina ceramics. Journal of Rare Earths, 2006, 24(1): 72–75.
[38] Li H, Hu K H, Liu Y S, et al. Improved mechanical properties of silica ceramic cores prepared by 3D printing and sintering processes. Scripta Materialia, 2021, 194: 113665.
[39] An X L, Mu Y H, Chen J W, et al. Compositional optimization of high-solid-loading ceramic cores via 3D printing. Additive Manufacturing, 2022, 58: 103054.
[40] Zhang K Q, He R J, Ding G J, et al. Effects of fine grains and sintering additives on stereolithography additive manufactured Al_2O_3 ceramic. Ceramics International, 2021, 47(2): 2303–2310.
[41] Hu K H, Wei Y M, Lu Z G, et al. Design of a shaping system for stereolithography with high solid loading ceramic suspensions. 3D Printing and Additive Manufacturing, 2018, 5(4): 311–318.
[42] Yin Y H, Wang J, Huang Q Q, et al. Influence of debinding parameter and nano-ZrO_2 particles on the silica-based ceramic cores fabricated by stereolithography-based additive manufacturing. Ceramics International, 2023, 49(12): 20878–20889.
[43] Gu Y, Duan W Y, Wang T C, et al. Additive manufacturing of Al_2O_3 ceramic core with applicable microstructure and mechanical properties via digital light processing of high solid loading slurry. Ceramics International, 2023, 49(15): 25216–25224.
[44] Ganesh V, Nandita G, Himanshu K. A study of ceramic core for investment casting. Advances in Materials and Mechanical Engineering, 2021: 379–389.
[45] Wu L, He J, Zeng H, et al. Research progress of manufacturing process on silica-based ceramic core. Dongfang Turbine, 2017: 54–59. (In Chinese)
[46] Bae C J, Kim D, Halloran J W. Mechanical and kinetic studies on the refractory fused silica of integrally cored ceramic mold fabricated by additive manufacturing. Journal of the European Ceramic Society, 2019, 39(2–3): 618–623.
[47] Zhang J, Yu K B, Wu J M, et al. Effects of $ZrSiO_4$ content on properties of SiO_2-based ceramics prepared by digital light processing. Ceramics International, 2023, 49(6): 9584–9591.
[48] Wang L Y, Hon M H. The effect of cristobalite seed on the crystallization of fused silica based ceramic core – A kinetic study. Ceramics International, 1995, 21(3): 187–193.
[49] Wilson P J, Blackburn S, Greenwood R W, et al. The role of zircon particle size distribution, surface area and contamination on the properties of silica-zircon ceramic materials. Journal of the European Ceramic Society, 2011, 31(9): 1849–1855.
[50] Kang H F, Li F, Zhao Y J, et al. Research status on ceramic cores and shells for superalloy hollow blades inveatment casting. Journal of Materials Engineering, 2013.
[51] Niu S X, Xu X Q, Li X, et al. Enhanced properties of silica-based ceramic cores by controlled particle sizes of cristobalite seeds. Advances in Applied Ceramics, 2019, 118(7): 403–408.
[52] Zhao X Z. Preparison and application of ceramic shell mold. Beijing Science and Technology Pulishing Co., Ltd., Beijing, 2021. (In Chinese)